ACS APPLIED ENERGY MATERIALS

www.acsaem.org

Letter

Catalysis of the Oxygen-Evolution Reaction in 1.0 M Sulfuric Acid by Manganese Antimonate Films Synthesized via Chemical Vapor Deposition

Jacqueline A. Dowling,[⊥] Zachary P. Ifkovits,[⊥] Azhar I. Carim, Jake M. Evans, Madeleine C. Swint, Alexandre Z. Ye, Matthias H. Richter, Anna X. Li, and Nathan S. Lewis*

Cite This: ACS Appl. Energy Mater. 2024, 7, 4288−4293

Read Online

ACCESS | Metrics & More | Article Recommendations | Supporting Information

ABSTRACT: Manganese antimonate ($Mn_ySb_{1-y}O_x$) electrocatalysts for the oxygen-evolution reaction (OER) were synthesized via chemical vapor deposition. Mn-rich rutile $Mn_{0.63}Sb_{0.37}O_x$ catalysts on fluorine-doped tin oxide (FTO) supports drove the OER for 168 h (7 days) at 10 mA cm^{-2} with a time-averaged overpotential of 687 ± 9 mV and with >97% Faradaic efficiency. Time-dependent anolyte composition analysis revealed the steady dissolution of Mn and Sb. Extended durability analysis confirmed that Mn-rich $Mn_ySb_{1-y}O_x$ materials are more active but dissolve at a faster rate than previously reported Sb-rich $Mn_ySb_{1-y}O_x$ alloys.

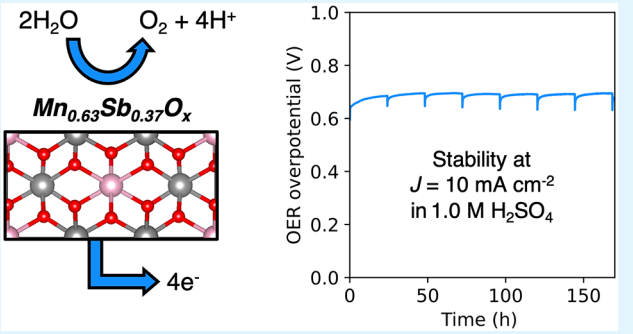

KEYWORDS: *electrolysis, oxygen-evolution reaction in acid, manganese antimony oxide, earth-abundant materials, heterogeneous catalysis, chemical vapor deposition*

The electrochemical oxygen-evolution reaction (OER) is an anodic process that oxidizes water, an abundant feedstock, and can supply electrons necessary to drive many fuel-forming cathodic processes including the production of H_2 from H_2O, NH_3 from N_2, and hydrocarbons from CO_2.[1−3] Water electrolysis for H_2 generation specifically is of interest in the storage of energy from intermittent renewable sources.[4,5] Carbon-free electricity can drive water electrolysis to generate green H_2 for use on demand.[6,7] Commercial proton-exchange membrane (PEM) electrolyzers use Ir-based catalysts to effect the oxygen-evolution reaction (OER) in acidic media.[8,9] IrO_x exhibits high OER activity and durability, but the low crustal abundance of Ir is a barrier to scale.[10−14] An earth-abundant, but less-active, electrocatalyst may be an acceptable replacement for IrO_x in scenarios with infrequent electrolyzer use and low-cost electricity.[10] Electrolyzers paired with seasonal or multiyear H_2 storage in reliable wind and solar systems may operate at reduced capacity factors (∼50%) and capitalize on abundant, otherwise-curtailed, zero-cost electricity to drive electrolysis.[5,10,15]

A variety of earth-abundant materials have displayed relatively stable oxygen-evolution catalysis in acidic aqueous electrolytes, including Mn-oxyhalides, arc-melted Ni_2Ta electrodes, Co-doped Fe_2O_3 thin films, and N_2-doped W-carbide nanoarrays.[16−19] Earth-abundant Mn-rich rutile $Mn_ySb_{1-y}O_x$ powders are effective catalysts for chemical oxygen-evolution in acidic media, and Sb-rich rutile $Mn_ySb_{1-y}O_x$ sputtered films have shown promising long-term durability.[20,21] Rutile $Mn_ySb_{1-y}O_x$ ($0.3 < y < 0.7$) materials are more active and stable than nonrutile $Mn_ySb_{1-y}O_x$ materials.[20−25] In this work, $Mn_{0.63}Sb_{0.37}O_x$ was synthesized via chemical vapor deposition (CVD). CVD is a scalable synthetic method and may be an effective approach to controllably coat catalyst layers onto high surface-area supports, including those suitable for use in a PEM electrolyzer.[26] The CVD deposition method complements previous synthetic routes for generation of $Mn_ySb_{1-y}O_x$ including sputtering, bulk powder mixing, and electrodeposition.[20−23]

$Mn_{0.63}Sb_{0.37}O_x$ thin films were deposited by CVD on fluorine-doped tin oxide (FTO) substrates using 30 supercycles that each consisted of 10 SbO_x subcycles and 5 MnO_x subcycles (Scheme 1).[27] Each chemical vapor deposition subcycle consisted of a precursor pulse with either tris(dimethylamido)antimony(III) (TDMA-Sb) or bis(ethylcyclopentadienyl)-manganese ($Mn(EtCp)_2$), in addition to an ozone coreactant pulse. The growth rates of MnO_x and SbO_x were independently measured via ellipsometry (Figure

Received: January 17, 2024
Revised: March 21, 2024
Accepted: March 21, 2024
Published: March 25, 2024

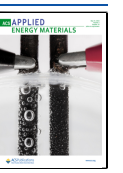

Scheme 1. (A) Synthesis of Crystalline $Mn_{0.63}Sb_{0.37}O_x$ via Chemical Vapor Deposition and Annealing. (B) Ternary Chemical Vapor Deposition with TDMA-Sb and $Mn(EtCp)_2$ Precursors, in Addition to Ozone As a Coreactant

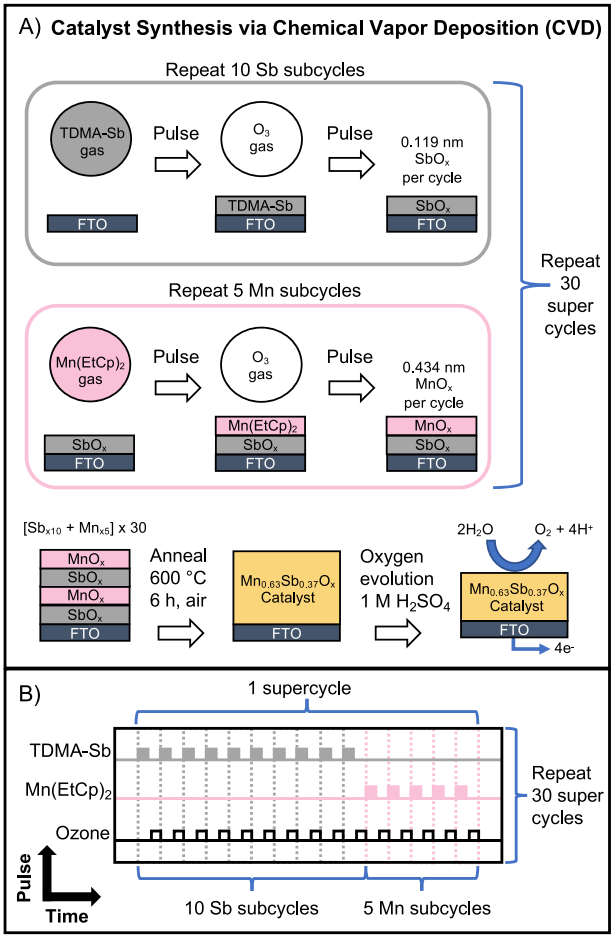

1A). The MnO_x thickness increased linearly with pulse duration, indicating controlled chemical vapor deposition, whereas the thickness of the SbO_x was constant regardless of the pulse duration, indicating self-limiting atomic-layer deposition.[28] The Mn−Sb binary oxide was formed using a 0.33 s pulse of $Mn(EtCp)_2$, which corresponded to 0.43 nm of MnO_x per cycle, and a 1 s pulse of TDMA-Sb, which corresponded to 0.12 nm of SbO_x per cycle. Inductively coupled plasma mass spectrometry (ICP-MS) indicated that the composition of the as-deposited, unannealed catalyst was Mn/(Mn+Sb) = 0.63 ± 0.01. After annealing in air for 6 h at the maximum tolerable temperature (600 °C) of the TEC8 FTO substrate, grazing incidence X-ray diffraction (GIXRD) analysis of $Mn_{0.64}Sb_{0.36}O_x$ showed reflections at $2\theta \approx 27°$, 35°, 53°, and 56°, consistent with a rutile crystal structure based on a comparison to the reflections of rutile $MnSb_2O_6$.[20,21,23]

A $Mn_{0.63}Sb_{0.37}O_x$ electrode was subjected to a 168 h (7 day) durability test at J = 10 mA cm^{-2} in 1.0 M H_2SO_4(aq), and the OER overpotential (η) was recorded (Figure 2A). During this experiment, the galvanostatic hold was interrupted at 24 h intervals, and voltammetric and impedance data were collected after 30 s at open circuit (Figure 2B and Figure S2). The measured overpotentials at J = 10 mA cm^{-2} were reduced by ∼14 mV to correct for the uncompensated ohmic resistance intrinsic to the electrochemical cell configuration. The time-

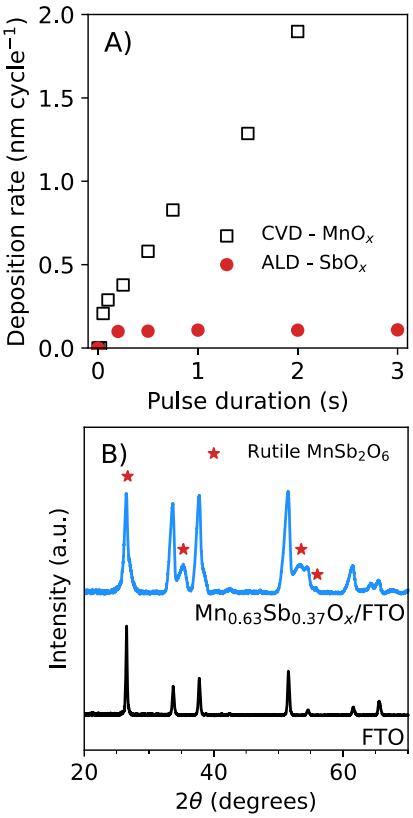

Figure 1. (A) Growth rates of MnO_x and SbO_x via CVD and ALD, respectively, derived from the analysis of ellipsometry data. (B) Grazing incidence X-ray diffraction (GIXRD) data acquired from $Mn_{0.64}Sb_{0.36}O_x$ and XRD data acquired from the TEC8 FTO substrate after annealing in air for 6 h at 600 °C.

averaged OER overpotential over the entire test duration was η = 687 ± 9 mV (the blue shaded region in Figure 2A shows the standard deviation). However, consistent with previous results for $Mn_ySb_{1-y}O_x$, during the short periods at open circuit, as well as between the first and second voltametric cycles collected in succession at each 24 h interval, the OER overpotential decreased and the catalyst "recovered" (Figure 2A, Figure S2B).[21,23] The OER overpotential at 10 mA cm^{-2} as measured from the voltammetric analyses was η = 617 mV at t = 0 h and was η = 618 mV at t = 168 h (Figure 2B, Figure S2B). Redox waves centered at 1.46 V vs the reversible hydrogen electrode (RHE) appeared and increased in magnitude, during the extended durability test (Figure 2B, Figure S2A), analogous to the behavior of $Mn_ySb_{1-y}O_x$ electrocatalysts deposited by sputtering.[21]

Aliquots of the electrolyte solution were taken without replacement at ∼24 h intervals, and the dissolution of Sb and Mn was measured by ICP-MS during the durability test at 10 mA cm^{-2} in 1.0 M H_2SO_4(aq) (Figure 2C). The average rate of Sb dissolution (11 weight % per day, or 0.0013 μmol cm^{-2} h^{-1}) was comparable to the average rate of Mn dissolution (8% per day, or 0.0015 μmol cm^{-2} h^{-1}) (Figure S3). The dissolution rate of both metals was lower during the initial 48 h of the test than at later time points. Another $Mn_{0.63}Sb_{0.37}O_x$ electrode from the same deposition batch yielded an average of 97.6% Faradaic efficiency for oxygen evolution during 93 h of continuous operation at 10 mA cm^{-2} in 1.0 M H_2SO_4 (Figure 2D). Hence, despite the high Faradaic efficiency and a relatively stable OER overpotential, substantial

https://doi.org/10.1021/acsaem.4c00135
ACS Appl. Energy Mater. 2024, 7, 4288−4293

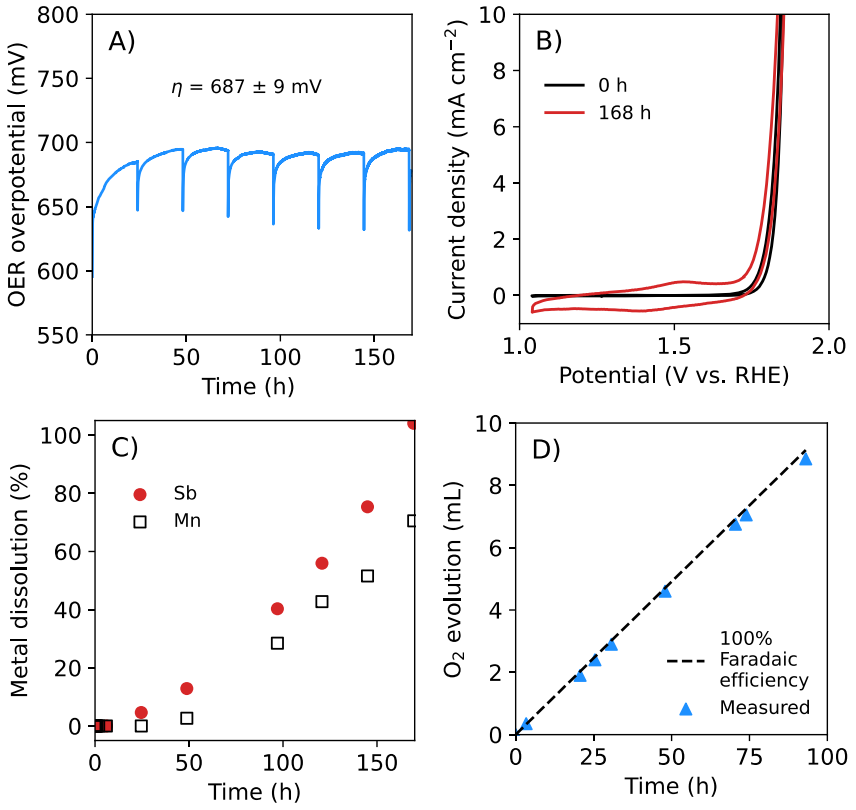

Figure 2. Electrochemical activity, stability, and Faradaic efficiency of $Mn_{0.63}Sb_{0.37}O_x$ during the OER at J = 10 mA cm^{-2} for 168 h (7 days) in 1.0 M H_2SO_4(aq). (A) Time dependence of the OER overpotential after correction for the uncompensated resistance of the cell. (B) Cyclic voltammograms (ν = 40 mV s^{-1}) collected after t = 0 h and after t = 168 h of the galvanostatic hold. (C) Amount of dissolved metal in the anolyte as quantified by ICP-MS, as a percentage of the total deposited Sb and total deposited Mn. (D) Eudiometric measurement of the level of O_2(g) production.

catalyst corrosion occurred, consistent with the behavior of sputtered Mn-rich alloys.[23,24] The OER overpotential and metal dissolution rates of a replicate electrode that was tested for 176 h (>7 days) at 10 mA cm^{-2} in 1.0 M H_2SO_4 were in agreement with that of the $Mn_{0.63}Sb_{0.37}O_x$ electrode described above (Figure S3).

An additional $Mn_{0.63}Sb_{0.37}O_x$ electrode was operated galvanostatically at J = 100 mA cm^{-2} and was subjected to very positive potentials during voltametric analysis (Figure 3). The time-averaged OER overpotential over a period of 8.5 h at J = 100 mA cm^{-2} was 724 ± 8 mV (Figure 3). Figure S8 presents an expanded view of the data in Figure 3 during the first 8 h of operation. The overpotential of the OER at J = 100 mA cm^{-2} was 709 mV at t = 0 h and 688 mV at t = 8 h (Figure 3). In the first 8 h at J = 100 mA cm^{-2} in 1.0 M H_2SO_4, ICP-MS indicated more leaching of Sb than of Mn (Figure 3C). The chronopotentiometry experiment at 100 mA cm^{-2} in 1.0 M H_2SO_4 was continued for 26 h, with periodic interruptions due to bubble formation that inhibited current flow at the counter electrode (Figure 3). Voltammetric analysis indicated that the initial OER overpotential at J = 350 mA cm^{-2} was 819 mV in 1.0 M H_2SO_4 (Figure S9).

The $Mn_{0.63}Sb_{0.37}O_x$ electrode was characterized before and after the 168 h of the OER durability test at J = 10 mA cm^{-2} in 1.0 M H_2SO_4(aq) by scanning electron microscopy (SEM), electrochemical impedance spectroscopy (EIS), energy dispersive X-ray spectroscopy (EDX), and X-ray photoelectron spectroscopy (XPS). The SEM data showed a conformal coating of the catalyst on the substrate prior to the OER, and EIS measurements (Figure S4B and C, respectively) indicated an ∼22-fold increase in surface roughness during the 168 h durability test (Figure S5). Notably, although the material dissolved, the overpotential required to produce J = 10 mA cm^{-2} did not change substantially during this time.

The redox waves observed at ∼1.46 V vs RHE (Figure 2B) in the voltammetric data are consistent with behavior of MnO_x and other $Mn_ySb_{1-y}O_x$ materials.[21,29] XP spectra of the $Mn_{0.63}Sb_{0.37}O_x$ catalyst material acquired before and after the 168 h OER durability test at J = 10 mA cm^{-2} in 1.0 M H_2SO_4(aq) indicated that the material was always principally composed of Mn(III) with some Mn(IV) observable (∼20%) after operation, consistent with previous analysis of antimonate systems (Figure S6, Figure S7, Table S3).[23] Sb sites in binary oxide materials are inactive for the OER reaction,[21,23,24] consistent with the OER being localized on Mn sites and mediated by Mn redox events, with Sb^{5+} ions contributing to electrochemical stability.[21−23] Electrocatalytically inactive Sb^{5+} sites may stabilize Mn sites that actively effect the OER by inducing enhanced hybridization of the O p-orbital and Mn d-orbital.[23,24] The Mn metal fraction as indicated by energy-dispersive X-ray (EDX) spectroscopy decreased from 64 ± 5% before operation to 49 ± 7% after 168 h at J = 10 mA cm^{-2} (Figure S4A). XP spectra of the Sb 3d region indicated a shift from 3.2 to 5.0 in the Sb oxidation state (Figure S6, Figure S7C, and Table S3). Mn-rich alloys are thus expected to be less stable than Sb-rich alloys, consistent with the substantial metal dissolution of the $Mn_{0.63}Sb_{0.37}O_x$ catalysts observed during the multiday durability test (Figure 2). However, some degree of

https://doi.org/10.1021/acsaem.4c00135
ACS Appl. Energy Mater. 2024, 7, 4288−4293

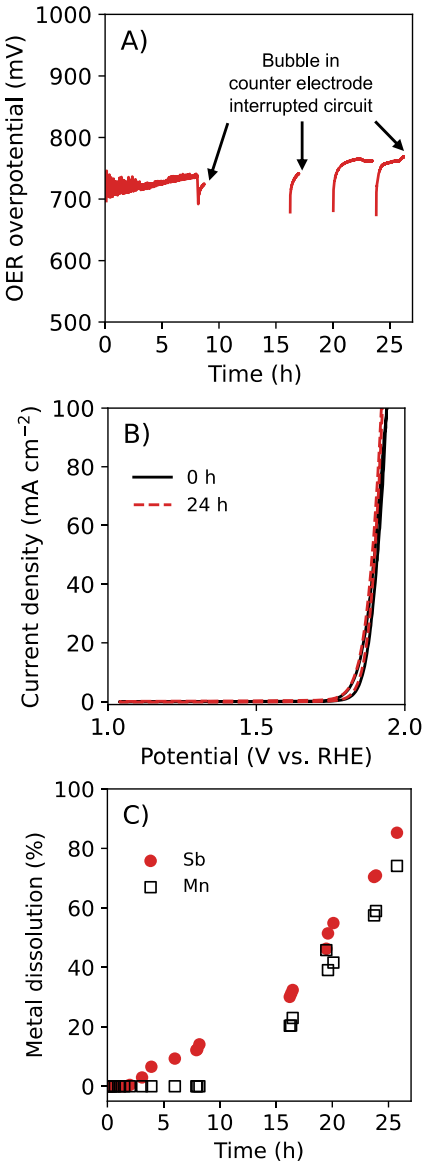

Figure 3. Electrochemical activity and stability of $Mn_{0.63}Sb_{0.37}O_x$ during OER at J = 100 mA cm^{-2} in 1.0 M H_2SO_4(aq). (A) Chronopotentiometric response. (B) Cyclic voltammograms collected initially as well as after 24 h under the galvanostatic hold. (C) Amount of dissolved metal in the anolyte as quantified by ICP-MS, presented as a percentage of the total deposited Sb and total deposited Mn.

electronic stabilization of Mn sites by Sb ions may account for the enhanced corrosion resistance observed herein relative to that reported for unary Mn oxide materials.[23,24]

In summary, the extended durability of rutile $Mn_{0.63}Sb_{0.37}O_x$ catalysts was assessed during galvanostatic operation at J = 10 mA cm^{-2} and at J = 100 mA cm^{-2} in 1.0 M H_2SO_4. After 168 h of operation at J = 10 mA cm^{-2}, a loss of electrocatalyst mass, an increase in porosity, and partial oxidation of the constituent Mn were observed relative to the as-prepared material. A lower overpotential was observed for the Mn-rich alloy at J = 10 mA cm^{-2} than previously reported for Sb-rich $Mn_ySb_{1-y}O_x$ alloys.[21] However, unlike the Sb-rich $Mn_ySb_{1-y}O_x$ alloys, $Mn_{0.63}Sb_{0.37}O_x$ catalysts corroded continuously during operation. This behavior is consistent with the notion that Sb stabilizes Mn sites, as well as with prior results on the behavior of Mn-rich alloys prepared by sputtering.[23,24] The extended duration testing reported here, along with previous reports, confirm an activity-stability trade-off across the Mn:Sb composition space.[30] A reduced Mn:Sb ratio may thus enhance the stability of $Mn_ySb_{1-y}O_x$ catalysts in acidic OER conditions while, however, producing a reduction in the OER activity. Despite the continuous corrosion of both Sb and Mn from the as-prepared material, the OER overpotential at J = 10 mA cm^{-2} did not substantially increase, even at the point that >90% of the catalyst mass had dissolved.

■ ASSOCIATED CONTENT

Supporting Information

The Supporting Information is available free of charge at https://pubs.acs.org/doi/10.1021/acsaem.4c00135.

Detailed experimental procedures, materials and chemicals, sample preparation, electrochemical measurements, materials characterization, additional OER overpotential data and metal dissolution rates, scanning electron micrographs, energy-dispersive X-ray spectroscopy data, X-ray diffraction data, and X-ray photoelectron spectra (PDF)

■ AUTHOR INFORMATION

Corresponding Author

Nathan S. Lewis − *Division of Chemistry and Chemical Engineering and Beckman Institute, California Institute of Technology, Pasadena, California 91125, United States;* orcid.org/0000-0001-5245-0538; Email: nslewis@caltech.edu

Authors

Jacqueline A. Dowling − *Division of Chemistry and Chemical Engineering, California Institute of Technology, Pasadena, California 91125, United States;* orcid.org/0000-0001-5642-8960

Zachary P. Ifkovits − *Division of Chemistry and Chemical Engineering, California Institute of Technology, Pasadena, California 91125, United States;* orcid.org/0000-0003-2538-0794

Azhar I. Carim − *Division of Chemistry and Chemical Engineering and Beckman Institute, California Institute of Technology, Pasadena, California 91125, United States;* orcid.org/0000-0003-3630-6872

Jake M. Evans − *Division of Chemistry and Chemical Engineering, California Institute of Technology, Pasadena, California 91125, United States;* orcid.org/0000-0002-8721-5316

Madeleine C. Swint − *Division of Chemistry and Chemical Engineering, California Institute of Technology, Pasadena, California 91125, United States*

Alexandre Z. Ye − *Division of Chemistry and Chemical Engineering, California Institute of Technology, Pasadena, California 91125, United States*

Matthias H. Richter − *Division of Engineering and Applied Sciences, California Institute of Technology, Pasadena, California 91125, United States;* orcid.org/0000-0003-0091-2045

Anna X. Li − *Division of Engineering and Applied Sciences, California Institute of Technology, Pasadena, California 91125, United States;* orcid.org/0000-0002-3435-3651

Complete contact information is available at: https://pubs.acs.org/10.1021/acsaem.4c00135

https://doi.org/10.1021/acsaem.4c00135
ACS Appl. Energy Mater. 2024, 7, 4288−4293

Author Contributions

[⊥]J.A.D. and Z.P.I. contributed equally.

Notes

The authors declare the following competing financial interest(s): N.S.L. is a scientific founder of and consultant to H2U Technologies, a company developing catalysts and electrolyzers for the production of hydrogen.

■ ACKNOWLEDGMENTS

This work was supported by the U.S. Department of Energy, Office of Science, Office of Basic Science under Award Number DE-FG02-03-ER15483. ICP-MS data were collected at the Water and Environment Lab of the Resnick Sustainability Institute at the California Institute of Technology. XPS data were collected at the Molecular Materials Resource Center of the Beckman Institute at the California Institute of Technology.

■ REFERENCES

(1) Song, J.; Wei, C.; Huang, Z.-F.; Liu, C.; Zeng, L.; Wang, X.; Xu, Z. J. A Review on Fundamentals for Designing Oxygen Evolution Electrocatalysts. *Chem. Soc. Rev.* **2020**, *49*, 2196−2214.

(2) Ghavam, S.; Vahdati, M.; Wilson, I. A. G.; Styring, P. Sustainable Ammonia Production Processes. *Front. Energy Res.* **2021**, DOI: 10.3389/fenrg.2021.580808.

(3) Nitopi, S.; Bertheussen, E.; Scott, S. B.; Liu, X.; Engstfeld, A. K.; Horch, S.; Seger, B.; Stephens, I. E. L.; Chan, K.; Hahn, C.; Nørskov, J. K.; Jaramillo, T. F.; Chorkendorff, I. Progress and Perspectives of Electrochemical CO2 Reduction on Copper in Aqueous Electrolyte. *Chem. Rev.* **2019**, *119*, 7610−7672.

(4) MIT Energy Initiative. *The Future of Energy Storage*; Technical Report; Massachusetts Institute of Technology, 2022.

(5) Dowling, J. A.; Rinaldi, K. Z.; Ruggles, T. H.; Davis, S. J.; Yuan, M.; Tong, F.; Lewis, N. S.; Caldeira, K. Role of Long-Duration Energy Storage in Variable Renewable Electricity Systems. *Joule* **2020**, *4*, 1907−1928.

(6) Panchenko, V. A.; Daus, Yu. V.; Kovalev, A. A.; Yudaev, I. V.; Litti, Yu. V. Prospects for the Production of Green Hydrogen: Review of Countries with High Potential. *Int. J. Hydrog. Energy* **2023**, *48*, 4551−4571.

(7) Davis, S. J.; Lewis, N. S.; Shaner, M.; Aggarwal, S.; Arent, D.; Azevedo, I. L.; Benson, S. M.; Bradley, T.; Brouwer, J.; Chiang, Y.-M.; Clack, C. T. M.; Cohen, A.; Doig, S.; Edmonds, J.; Fennell, P.; Field, C. B.; Hannegan, B.; Hodge, B.-M.; Hoffert, M. I.; Ingersoll, E.; Jaramillo, P.; Lackner, K. S.; Mach, K. J.; Mastrandrea, M.; Ogden, J.; Peterson, P. F.; Sanchez, D. L.; Sperling, D.; Stagner, J.; Trancik, J. E.; Yang, C.-J.; Caldeira, K. Net-Zero Emissions Energy Systems. *Science* **2018**, *360*, eaas9793.

(8) Ayers, K. The Potential of Proton Exchange Membrane−Based Electrolysis Technology. *Curr. Opin. Electrochem.* **2019**, *18*, 9−15.

(9) Buttler, A.; Spliethoff, H. Current Status of Water Electrolysis for Energy Storage, Grid Balancing and Sector Coupling via Power-to-Gas and Power-to-Liquids: A Review. *Renew. Sustain. Energy Rev.* **2018**, *82*, 2440−2454.

(10) Hubert, M. A.; King, L. A.; Jaramillo, T. F. Evaluating the Case for Reduced Precious Metal Catalysts in Proton Exchange Membrane Electrolyzers. *ACS Energy Lett.* **2022**, *7*, 17−23.

(11) Riedmayer, R.; Paren, B. A.; Schofield, L.; Shao-Horn, Y.; Mallapragada, D. Proton Exchange Membrane Electrolysis Performance Targets for Achieving 2050 Expansion Goals Constrained by Iridium Supply. *Energy Fuels* **2023**, *37*, 8614−8623.

(12) Minke, C.; Suermann, M.; Bensmann, B.; Hanke-Rauschenbach, R. Is Iridium Demand a Potential Bottleneck in the Realization of Large-Scale PEM Water Electrolysis? *Int. J. Hydrog. Energy* **2021**, *46*, 23581−23590.

(13) Bernt, M.; Hartig-Weiß, A.; Tovini, M. F.; El-Sayed, H. A.; Schramm, C.; Schröter, J.; Gebauer, C.; Gasteiger, H. A. Current Challenges in Catalyst Development for PEM Water Electrolyzers. *Chem. Ing. Technol.* **2020**, *92*, 31−39.

(14) Cherevko, S.; Geiger, S.; Kasian, O.; Kulyk, N.; Grote, J.-P.; Savan, A.; Shrestha, B. R.; Merzlikin, S.; Breitbach, B.; Ludwig, A.; Mayrhofer, K. J. J. Oxygen and Hydrogen Evolution Reactions on Ru, RuO_2, Ir, and IrO_2 Thin Film Electrodes in Acidic and Alkaline Electrolytes: A Comparative Study on Activity and Stability. *Catal. Today* **2016**, *262*, 170−180.

(15) Ruggles, T. H.; Dowling, J. A.; Lewis, N. S.; Caldeira, K. Opportunities for Flexible Electricity Loads Such as Hydrogen Production from Curtailed Generation. *Adv. Appl. Energy* **2021**, *3*, No. 100051.

(16) Han, N.; Yang, K. R.; Lu, Z.; Li, Y.; Xu, W.; Gao, T.; Cai, Z.; Zhang, Y.; Batista, V. S.; Liu, W.; Sun, X. Nitrogen-Doped Tungsten Carbide Nanoarray as an Efficient Bifunctional Electrocatalyst for Water Splitting in Acid. *Nat. Commun.* **2018**, *9*, 924.

(17) Kwong, W. L.; Lee, C. C.; Shchukarev, A.; Messinger, J. Cobalt-Doped Hematite Thin Films for Electrocatalytic Water Oxidation in Highly Acidic Media. *Chem. Commun.* **2019**, *55*, 5017−5020.

(18) Mondschein, J. S.; Kumar, K.; Holder, C. F.; Seth, K.; Kim, H.; Schaak, R. E. Intermetallic Ni_2Ta Electrocatalyst for the Oxygen Evolution Reaction in Highly Acidic Electrolytes. *Inorg. Chem.* **2018**, *57*, 6010−6015.

(19) Pan, S.; Li, H.; Liu, D.; Huang, R.; Pan, X.; Ren, D.; Li, J.; Shakouri, M.; Zhang, Q.; Wang, M.; Wei, C.; Mai, L.; Zhang, B.; Zhao, Y.; Wang, Z.; Graetzel, M.; Zhang, X. Efficient and Stable Noble-Metal-Free Catalyst for Acidic Water Oxidation. *Nat. Commun.* **2022**, *13*, 2294.

(20) Ifkovits, Z. P.; Evans, J. M.; Kempler, P. A.; Morla, M. B.; Pham, K. H.; Dowling, J. A.; Carim, A. I.; Lewis, N. S. Powdered $Mn_ySb_{1-y}O_x$ Catalysts for Cerium-Mediated Oxygen Evolution in Acidic Environments. *ACS Energy Lett.* **2022**, *7*, 4258−4264.

(21) Moreno-Hernandez, I. A.; MacFarland, C. A.; Read, C. G.; Papadantonakis, K. M.; Brunschwig, B. S.; Lewis, N. S. Crystalline Nickel Manganese Antimonate as a Stable Water-Oxidation Catalyst in Aqueous 1.0 M H_2SO_4. *Energy Environ. Sci.* **2017**, *10*, 2103−2108.

(22) Evans, T. A.; Choi, K.-S. Electrochemical Synthesis and Investigation of Stoichiometric, Phase-Pure $CoSb_2O_6$ and $MnSb_2O_6$ Electrodes for the Oxygen Evolution Reaction in Acidic Media. *ACS Appl. Energy Mater.* **2020**, *3*, 5563−5571.

(23) Zhou, L.; Shinde, A.; Montoya, J. H.; Singh, A.; Gul, S.; Yano, J.; Ye, Y.; Crumlin, E. J.; Richter, M. H.; Cooper, J. K.; Stein, H. S.; Haber, J. A.; Persson, K. A.; Gregoire, J. M. Rutile Alloys in the Mn−Sb−O System Stabilize Mn^{3+} To Enable Oxygen Evolution in Strong Acid. *ACS Catal.* **2018**, *8*, 10938−10948.

(24) Luke, S.; Chatti, M.; Yadav, A.; Kerr, B. V.; Kangsabanik, J.; Williams, T.; Cherepanov, P. V.; Johannessen, B.; Tanksale, A.; MacFarlane, D. R.; Hocking, R. K.; Alam, A.; Yella, A.; Simonov, A. N. Mixed Metal−Antimony Oxide Nanocomposites: Low pH Water Oxidation Electrocatalysts with Outstanding Durability at Ambient and Elevated Temperatures. *J. Mater. Chem. A* **2021**, *9*, 27468−27484.

(25) Shinde, A.; Jones, R. J. R.; Guevarra, D.; Mitrovic, S.; Becerra-Stasiewicz, N.; Haber, J. A.; Jin, J.; Gregoire, J. M. High-Throughput Screening for Acid-Stable Oxygen Evolution Electrocatalysts in the $(Mn−Co−Ta−Sb)O_x$ Composition Space. *Electrocatalysis* **2015**, *6*, 229−236.

(26) Laube, A.; Hofer, A.; Ressel, S.; Chica, A.; Bachmann, J.; Struckmann, T. PEM Water Electrolysis Cells with Catalyst Coating by Atomic Layer Deposition. *Int. J. Hydrog. Energy* **2021**, *46*, 38972−38982.

(27) Mackus, A. J. M.; Schneider, J. R.; MacIsaac, C.; Baker, J. G.; Bent, S. F. Synthesis of Doped, Ternary, and Quaternary Materials by Atomic Layer Deposition: A Review. *Chem. Mater.* **2019**, *31*, 1142−1183.

(28) Yang, R. B.; Bachmann, J.; Reiche, M.; Gerlach, J. W.; Gösele, U.; Nielsch, K. Atomic Layer Deposition of Antimony Oxide and Antimony Sulfide. *Chem. Mater.* **2009**, *21*, 2586−2588.

(29) McCrory, C. C. L.; Jung, S.; Ferrer, I. M.; Chatman, S. M.; Peters, J. C.; Jaramillo, T. F. Benchmarking Hydrogen Evolving

Reaction and Oxygen Evolving Reaction Electrocatalysts for Solar Water Splitting Devices. *J. Am. Chem. Soc.* **2015**, *137*, 4347−4357.
(30) Dowling, J. A. Long-Duration Energy Storage in Reliable Wind and Solar Electricity Systems. Ph.D. Dissertation, California Institute of Technology, Pasadena, CA, 2023.

https://doi.org/10.1021/acsaem.4c00135
ACS Appl. Energy Mater. 2024, 7, 4288−4293